A Resolution Enhancement Technique for Ultrafast Coded Medical Ultrasound

Denis Bujoreanu
Creatis, Univ.Lyon, INSALyon, UCB Lyon 1, UJM-Saint Etienne, CNRS, Inserm, Lyon, France
denis.bujoreanu@creatis.insa-lyon.fr

Yanis Mehdi Benane
Creatis, Univ.Lyon, INSALyon, UCB Lyon 1, UJM-Saint Etienne, CNRS, Inserm, Lyon, France
yanis.benane@creatis.insa-lyon.fr

Hervé Liebgott
Creatis, Univ.Lyon, INSALyon, UCB Lyon 1, UJM-Saint Etienne, CNRS, Inserm, Lyon, France
liebgott@creatis.insa-lyon.fr

Barbara Nicolas
Creatis, Univ.Lyon, INSALyon, UCB Lyon 1, UJM-Saint Etienne, CNRS, Inserm, Lyon, France
barbara.nicolas@creatis.insa-lyon.fr

Olivier Basset
Creatis, Univ.Lyon, INSALyon, UCB Lyon 1, UJM-Saint Etienne, CNRS, Inserm, Lyon, France
olivier.basset@creatis.insa-lyon.fr

Denis Friboulet
Creatis, Univ.Lyon, INSALyon, UCB Lyon 1, UJM-Saint Etienne, CNRS, Inserm, Lyon, France
denis.friboulet@creatis.insa-lyon.fr

***Abstract*—In the quest for faster ultrasound image acquisition rate, low echo signal to noise ratio is often an issue. Binary Phase Shift Keyed (BPSK) Golay codes have been implemented in a large number of imaging methods, and their ability to increase the image quality is already proven. In this paper we propose an improvement of the BPSK modulation, where the effect of the narrow-band ultrasound probe, used for acquisition, is compensated. The optimized excitation signals are implemented in a Plane Wave Compounding (PWC) imaging approach. Simulation and experimental results are presented. Numerical studies show 41% improvement of axial resolution and bandwidth, over the classical BPSK modulated Golay codes. Experimental acquisitions on cyst phantom show an improvement of image resolution of 32%. The method is also compared to classical pulse (small wave packets) emission and 25% boost of resolution is achieved for a $6dB$ higher echo signal to noise ratio. The experimental results obtained using UlaOp 256 prove the feasibility of the method on a research scanner while the theoretical formulation shows that the optimization of the excitation signals can be applied to any binary sequence and does not depend on the emission/reception beamforming.**

***Index Terms*—Golay sequences, BPSK, Resolution enhancement compression, plane wave imaging**

I. Introduction

Perhaps one of the most challenging tasks in present-day ultrasound image reconstruction research is to find a way of increasing the frame acquisition rate without loss of image quality. Since the introduction of ultrasound scanners, numerous emission/reception beamforming schemes that increase the frame rate (comparing to focused beam ultrasound) have been proposed such as: synthetic aperture imaging [1], diverging wave [2] and plane wave imaging [3]. Since all of these techniques employ wide beam insonifications of the imaged medium, the signal to noise ratio of the backscattered echoes is decreased compared to focused ultrasound thus a lower image quality is obtained. To overcome this issue, one can increase the number of active elements in emission (for synthetic aperture) or the number of diverging/plane wave insonifications. Another solution for this issue is to use excitation signals that carry more energy such as: pseudo-orthogonal codes [4]–[6], chirps [7], [8] or a mix between codes and chirps [9]. Complementary Golay sequences have been already implemented in ultrasound imaging [9]–[12] and their ability to increase the echo signal to noise ratio after the pulse compression step was proven. However as it was shown in [10] the maximum axial resolution achievable is reached when the Golay sequences modulation assigns a sequence bit to a single cycle of a sinusoid (centered at the middle frequency of the probe), regardless of the bandwidth of the employed ultrasound probe.

In this work, we propose an Optimized Golay Coded (OGC) approach that allows to increase the image resolution achievable by the ultrasound imaging methods employing Golay coding. The main idea behind our approach is to combine Binary Phased Shift Keyed (BPSK) excitations with a technique that boosts the bandwidth of the employed ultrasound probe [7] called "Resolution enhancement compression". The designed excitation signals are emitted using a plane wave beamforming approach. Furthermore, we discuss the generalization of the approach on any family of binary sequences (m-sequences, Gold, Kasami).

II. Methods

A. Plane Wave Compounding (PWC)

Since, as we will show further in this paper, the ability of our approach to boost the resolution does not depend on the emission/reception beamforming technique the choice of the emission scheme is trivial. For this work, we combined OGC with coherent Plane Wave Compounding (PWC), an imaging technique that only needs few insonifications to reconstruct a

This work was performed within the framework of the ANR-11 TecSan-00801 BBMUT and was supported by LABEX CELYA (ANR-10-LABX-0060) and LABEX PRIMES (ANR-10-LABX-0063), within the program "Investissements d'Avenir" (ANR-11-IDEX-0007) operated by the French National Research Agency (ANR).

ISBN 978-90-827970-1-5 © EURASIP 2018

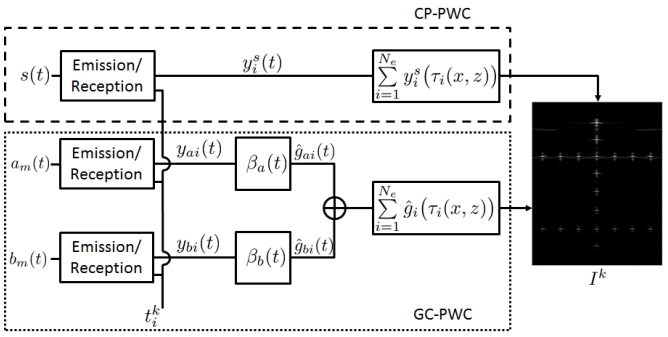

Fig. 1. Low resolution radiofrequency image reconstruction using: Classical Pulse Plane Wave Compounding (CP-PWC) (dashed box) and Golay Coded Plane Wave Compounding (GC-PWC) (dotted box). The DAS beamforming delays, $\tau_i(x,z)$ are given by (1) in [3]

full image of the medium [3]. In PWC, each plane wave k is emitted with a steering angle equal to:

$$\alpha^k = arcsin\big(\frac{k\lambda}{x_{lat}}\big), k \in \{-N_{pw}/2, \cdots, N_{pw}/2-1\} \quad (1)$$

where N_{pw} is the total number of waves to be emitted. From (1), the emission delays of the plane wave k for each element i of the transducer can be deduced, $t_i^k = (i-1)pitch \times tan(\alpha_k)/c$, where $pitch$ represents the distance between the center of two elements of the probe and c is the propagation speed of the ultrasound wave in soft tissues.

The reconstruction pipeline for a single low resolution CP-PWC image (I^k) is represented in the Fig1, where $s(t)$ is the excitation signal (1-3 sinusoid cycles) and $y_i(t)$ are the backscattered echoes received by the i^{th} element of the probe. The final CP-PWC image (I) is obtained by coherently adding all the N_{pw} low resolution images I^k. Lastly, envelope extraction and log compression is applied to I.

B. Golay encoded scheme (GC-PWC)

What makes Golay sequences suitable for ultrasound application is their complementarity property, which allows pulse compression with limited side lobe levels. Let us suppose a and b to be a pair of Golay binary sequences of length n bits: $a = a_0, a_1, \cdots, a_{n-1}$ and $b = b_0, b_1, \cdots, b_{n-1}$ with $a_j, b_j \in \{-1, 1\}$. Since a and b are complementary then:

$$R_{aa}(j) + R_{bb}(j) = 2n\delta(j) \quad (2)$$

where $R_{aa}(j)$ and $R_{bb}(j)$ represent the autocorrelation products of the sequence a and b respectively. $\delta(j)$ is the Kronecker delta function. In order to be able to emit a plane wave k that carries a corresponding sequence a or b, these binary codes need to be modulated at a central frequency inside the bandwidth of the ultrasound probe. Usually [9], [10] a Binary Phase Shift Keying (BPSK) modulation technique is employed. BPSK consists in shifting the phase of a sinusoid (called carrier) between two possible values 0 and π corresponding to the code bit to be sent 1 or -1. In [10] it was suggested that the best compromise between the echo to noise ratio and temporal resolution of the compressed waveforms is achieved when the carrier phase is updated every cycle (one sequence bit corresponds to one period of carrier sinusoid).

Let us suppose a band-limited ultrasound probe with a central frequency of $f_0 = 1/T_0$. The BPSK modulated Golay sequences $a_m(t)$ and $b_m(t)$ can be written as:

$$\begin{aligned} a_m(t) &= \sum_{i=0}^{n-1} a_i \delta\Big(t - iT_0\Big) * [cos(\tfrac{2\pi t}{T_0}) rect(\tfrac{t}{T_0})] \\ b_m(t) &= \sum_{i=0}^{n-1} b_i \delta\Big(t - iT_0\Big) * [cos(\tfrac{2\pi t}{T_0}) rect(\tfrac{t}{T_0})] \end{aligned} \quad (3)$$

where $rect(t)$ is the rectangular function. An example of a BPSK modulated Golay sequence is presented in Fig.2b. As showed in [9], from (2) and (3) the pulse compression of the signals $a_m(t)$ and $b_m(t)$ can be reduced to:

$$\begin{aligned} R_{a_m a_m}(t) + R_{b_m b_m}(t) = \Big[&(\tfrac{nT_0}{2} - n|t|) cos\big(\tfrac{2\pi t}{T_0}\big) \\ &- \tfrac{nT_0}{2\pi} sin\big(\tfrac{2\pi|t|}{T_0}\big)\Big] rect\big(\tfrac{t}{2T_0}\big) \end{aligned} \quad (4)$$

In (4), one can recognize that the compressed signal represents the autocorrelation product of one carrier period, and that no side-lobes are generated thanks to the $rect\big(\frac{t}{2T_0}\big)$ term.

A graphical representation of the Golay Coded Plane Wave Compounding (GC-PWC) image reconstruction pipeline is shown in Fig.1. One can observe that the data acquisition is performed in two steps for each of the plane wave k. First the signal $a_m(t)$ is emitted by the probe, with the delays t_i^k, and the backscattered echoes $y_{ai}(t)$ are recorded. Second the signal $b_m(t)$ is emitted with the same delays t_i^k, and the new backscattered echoes $y_{bi}(t)$ are recorded. In order to perform the next step which is pulse compression, one needs to make the hypothesis that the medium does not move between the two acquisitions, so the echoes of $a_m(t)$ and $b_m(t)$ are in-phase. The pulse compression is then performed by applying the corresponding matched filters $\beta_a(t) = a_m(-t)$ and $\beta_b(t) = b_m(-t)$ to the recorded signals $y_{ai}(t)$ and $y_{bi}(t)$ respectively. The compressed signals can be written as:

$$\hat{g}_i(t) = \hat{g}_{ai}(t) + \hat{g}_{bi}(t) = y_{ai}(t) * \beta_a(t) + y_{bi}(t) * \beta_b(t) \quad (5)$$

As showed in [5], the signals $y_{ai}(t)$ can be defined as $y_{ai}(t) = a_m(t) * g_i(t)$ were $g_i(t)$ is the pulsed plane wave response of the medium seen by the i^{th} element of the probe. Using (4) and the expression $y_{ai}(t)$, (5) becomes:

$$\hat{g}_i(t) = \big[R_{a_m a_m}(t) + R_{b_m b_m}(t)\big] * g_i(t) \quad (6)$$

From (6) and since $y_i^s(t) = s(t) * g_i(t)$ ($y_i^s(t)$ are the signals received in CP-PWC, cf. Fig.1), the "difference" between the echoes received in CP-PWC and the waveform of the GC-PWC compressed echoes is simply the "difference" between the signal $s(t)$ and $\big[R_{a_m a_m}(t) + R_{b_m b_m}(t)\big]$.

The signals $\hat{g}_i(t)$ are then first beamformed using Delay And Sum (DAS) algorithm and then compounded using in order to obtain the final image.

C. Optimized Golay encoded scheme (OGC-PWC)

Since each backscattered echo, after the compression using (5), yields a waveform as defined in (4), normally we should expect an image resolution equal to the width at half height of $\big[R_{a_m a_m}(t) + R_{b_m b_m}(t)\big]$ envelope. However, this is not the case, since during the emission and reception the signals are

ISBN 978-90-827970-1-5

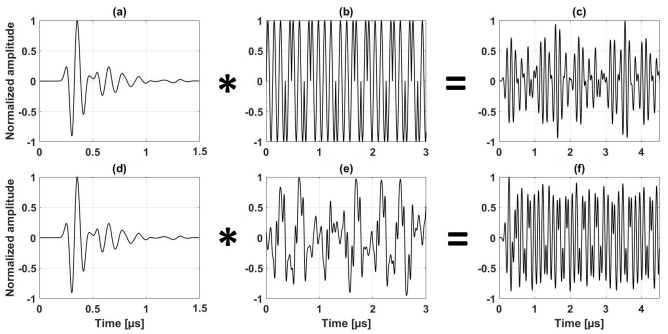

Fig. 2. a&d) - Pulse echo acousto-electrical impulse response of the ultrasound probe, b) - First 25 BPSK modulated bits of $a_m(t)$, c) - Convolution product of a BPSK modulated Golay sequence and the pulse echo acousto-electrical impulse response of the ultrasound probe ($a_m(t) * h_{er}(t)$), e) - First 25 BPSK modulated bits of $a^o_m(t)$, f) - Convolution product of a optimal modulated Golay sequence and the ulse echo acousto-electrical impulse response of the ultrasound probe ($a^o_m(t) * h_{er}(t)$). In this work $n = 128$, $(Hex)a$=EDE2ED1DEDE212E2EDE2ED1D121DED1D and $(Hex)b$=EDE2ED1DEDE212E2121D12E2EDE212E2.

convolved with the acousto-electrical impulse response ($h(t)$) of the ultrasound probe. $h(t)$ is usually band-limited thus the resolution of the image will be decreased. For the rest of this work, we will call the pulse-echo acousto-electrical impulse response of the probe the signal $h_{er}(t) = h(t) * h(t)$ (Fig.2a).

Let us suppose a scatterer at the medium position (x, z) defined by its reflectivity coefficient $\gamma(x, z)$. The echo that this scatterer generates (at the i^{th} element of the probe) when insonified with a plane wave that carries the signal $a_m(t)$ (or $b_m(t)$) can be defined as:

$$\begin{aligned} e_{ai}(t) &= \frac{\gamma(x,z)}{\sqrt{(x-x_i)^2+z^2}} a_m(t) * h_{er}(t) * \delta(t - \tau_i(x, z)) \\ e_{bi}(t) &= \frac{\gamma(x,z)}{\sqrt{(x-x_i)^2+z^2}} b_m(t) * h_{er}(t) * \delta(t - \tau_i(x, z)) \end{aligned} \tag{7}$$

where $\tau_i(x, z)$ is the forward/backward propagation time of the wave, between the probe, scatterer and i^{th} element position. In Fig.2c is shown the waveform $e_{ai}(t)$ (cropped to correspond to the first 25 modulated bits of $a_m(t)$). After compressing $e_{ai}(t)$ and $e_{bi}(t)$ using (5) we obtain:

$$\begin{aligned} \hat{e}_i(t) &= e_{ai}(t) * \beta_a(t) + e_{bi}(t) * \beta_b(t) \\ &= \eta \Big[\big(R_{a_m a_m}(t) + R_{b_m b_m}(t) \big) * h_{er}(t) \Big] * \delta(t - \tau_i(x, z)) \end{aligned} \tag{8}$$

with $\eta = \frac{\gamma(x,z)}{\sqrt{(x-x_i)^2+z^2}}$.

In Fig.3, we show the results of (8) and the expected result of pulse compression obtained using (4). As one can observe, the results of compression after the convolution with $h_{er}(t)$ yield a lower resolution (width at half height 46% larger) with

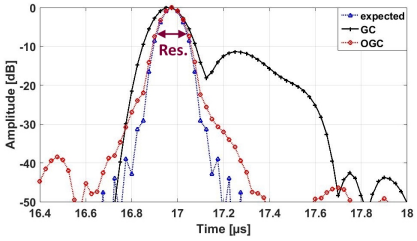

Fig. 3. Envelops of the expected, GC and OGC waveforms of the signal obtained after echo compression using (4), (8) and (11) respectively.

significant higher side-lobes (around $-11dB$). To overcome this drawback, in this work we propose to change the excitation signals $a_m(t)$ and $b_m(t)$ in such way so the pulse-echo acousto-electrical impulse response of the probe is compensated in the frequency bands where it is inefficient. This is the principle of Resolution enhancement compression which was successfully applied on chirp coded excitation in mono-element ultrasound imaging [7] and plane wave imaging [8]. To boost the bandiwdth of the ultrasound probe, we propose to deconvolve from the GC-PWC excitation signals, $a_m(t)$ and $b_m(t)$, the pulse-echo acousto-electrical impulse response of the elements $h_{er}(t)$. Thus, the excitation signals for OGC-OPT become:

$$\begin{aligned} a^o_m(f) &= a_m(f) \frac{h^*_{er}(f)}{|h_{er}(f)|^2 + \psi} \\ b^o_m(f) &= b_m(f) \frac{h^*_{er}(f)}{|h_{er}(f)|^2 + \psi} \end{aligned} \tag{9}$$

where $a_m(f)$, $b_m(f)$ and $h_{er}(f)$ are the Fourier transforms of the temporal signals $a_m(t)$, $b_m(t)$ and $h_{er}(t)$ respectively. $(.)^*$ represents the complex conjugate. In (9), the deconvolution is performed using a Wiener filter tunned with a parameter ψ. Indeed, ideally one would prefer to perform the deconvolution in (9) using an inverse filter $1/h_{er}(f)$, however since $h_{er}(f)$ is band-limited and the GC-excitation signals are broadband, the parameter ψ allows to bypass zero division and noise amplification. The trade-off of using ψ is that (9) will not yield the same resolution as an ideal inverse filter deconvolution.

OGC-PWC image reconstruction scheme follows exactly the same pipline as GC-PWC (Fig.1), the only difference being the excitation signals, switched to $a^o_m(t)$ and $b^o_m(t)$. In this case, the echoes $e^o_{ai}(t)$ and $e^o_{bi}(t)$ generated at the medium point (x, y) can be written as:

$$\begin{aligned} e^o_{ai}(t) &= \eta a^o_m(t) * h_{er}(t) * \delta(t - \tau_i(x, z)) \\ e^o_{bi}(t) &= \eta b^o_m(t) * h_{er}(t) * \delta(t - \tau_i(x, z)) \end{aligned} \tag{10}$$

From (9) and (10) it can we obtain:

$$\begin{aligned} \hat{e}^o_i(t) &= e^o_{ai}(t) * \beta_a(t) + e^o_{bi}(t) * \beta_b(t) \\ &\approx \eta \Big[R_{a_m a_m}(t) + R_{b_m b_m}(t) \Big] * \delta(t - \tau_i(x, z)) \end{aligned} \tag{11}$$

For explicit values of ψ: $\psi << |h_{er}(f)|, \forall f \in [f_0 - B/2, f_0 + B/2]$ and $\psi >> |h_{er}(f)|, \forall f \notin (f_0 - B/2, f_0 + B/2)$ where B is the ultrasound probe bandwidth. The result of echo compression using (11) is presented in Fig.3, where it can be distinctly seen that OGC compression improves the width at half height by 43% compared to GC compression and its only 3% short from reaching the expected theoretical value. Moreover, OGC improves also the compression side-lobes, higher side-lobe being only around $-40dB$.

III. Simulation results

In order to assess the ability of the proposed method to increase the ultrasound image quality, a numerical study was performed using FieldII [13] on two types of phantoms from the Plane-wave Imaging Challenge in Medical UltraSound (PICMUS) dataset [14] . A numerical model of the ultrasound LA523E (Esaote, Florence, Italy) was used. The probe's parameters were: $pitch = 0.245mm$, $f_0 = 8.5MHz$, $N_{el} = 192$

ISBN 978-90-827970-1-5 © EURASIP 2018

active elements and a pulse-echo acousto-electrical impulse response $h_{er}(t)$ (Fig.2a). $N_{pw} = 9$ plane waves (equally spaced between $(-7°, 7°)$), each steered following (1) were used to insonify the medium. $20dB$ additive white Gaussian noise $(n(t))$ was added to the received backscattered echoes in order to reproduce at best the experimental conditions.

The following image quality metrics were studied:

(a) **Axial resolution**—width at half height of the point spread function generated by a single scatterer

(b) **Bandwidth**—the frequency span of the $y_i(t)$ signals for CP-PWC and of the $\hat{y}_i(t)$ signals for GC-PWC and OGC-PWC. Larger bandwidths corresponding to better axial resolution and thinner speckle in the ultrasound image

(c) **eSNR**—echo signal to noise ratio, measured on the $y_i(t)$ signals for CP-PWC and on the $\hat{y}_i(t)$ signals for GC-PWC and OGC-PWC

$$eSNR = 10log\Big(\frac{E\{|\hat{y}_i(t)|^2\}}{E\{|\hat{n}_i(t)|^2\}}\Big) \tag{12}$$

(d) **CNR**—Contrast to noise ratio that quantifies the perceived difference between a target ROI of the image and its background

$$CNR = \frac{|\mu_{ROI} - \mu_{back}|}{\sqrt{\sigma^2_{ROI} + \sigma^2_{back}}} \tag{13}$$

where μ_{ROI} (μ_{back}) and σ_{ROI} (σ_{back}) are the average and the variance of the intensity inside (outside) the target ROI.

(e) **Auto-correlation length in the axial direction (ACL)**—measure obtained using:

$$ACL[m, j] = \sum_{i=-\infty}^{\infty} I[j, i + m]I[j, i] \tag{14}$$

where I is the beamformed image (after compounding and before envelope extraction). m and j are the indexes of the vertical and horizontal lines respectively. Smaller width at half height of ACL implies samaller speckle in the axial direction of the image.

A. Resolution phantom results

In Fig.4 are presented the B-mode images obtained using CP, GC and OGC -PWC respectively. In Fig.4a and b one can observe that the overall image quality provided by GC-PWC and CP-PWC are very similar. This result is also proved by the envelope of Point Spread Function (PSF) of the scatterer placed at the medium position $(x, z) = (0, 30)mm$ represented

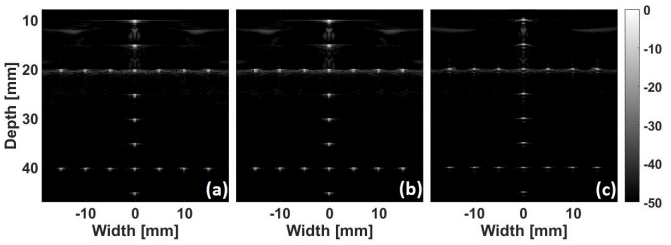

Fig. 4. B-mode images of the PICMUS resolution phantom, obtained using 9 plane wave compounding for: a) - CP-PWC, b) - GC-PWC, c) - OGC-PWC

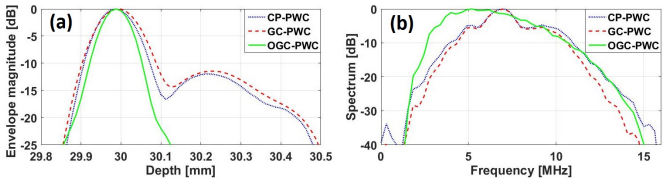

Fig. 5. a) - Envelope magnitude and b) - Bandwidth of the scatterer placed at $(x, z) = (0, 30)mm$

in Fig.5. OGC-PWC image (Fig.4c) and scatterer PSF (Fig.5), shows however improved image resolution, while no compression side-lobes are being generated in the image. The image resolution, bandwidths and $eSNR$ measures for the three methods are summed up in the Table I.

	Axial Res.	***Bandwidth***	***eSNR***
CP-PWC	$128.9\mu m$	$5.13MHz$	$21dB$
GC-PWC	$143.3\mu m$	$4.59MHz$	$38dB$
OGC-PWC	$101.6\mu m$	$6.49MHz$	$33dB$
OGC vs CP	$+27\%$	27%	$+12dB$
OGC vs GC	$+41\%$	41%	$-5dB$

TABLE I

The results in Table I show improvements for OGC-PWC for all metrics except $eSNR$. However, these $eSNR$ results are coherent with the expected values since, a Golay excitation scheme yields an $eSNR$ boost of $10log(n) = 10log(128) = 21dB$ [11] as compared to CP-PWC. The $eSNR$ decrease of $5dB$ between GC-PWC and OGC-PWC is also expected since, as one can see in Fig.1b and Fig.1e the excitation signal is more energetic for GC-PWC than for OGC-PWC (by $4.77dB$).

The bandwidth measurements (Fig.5b) on the compressed signals also show an improvement of OGC-PWC $(6.49MHz)$ compared to GC-PWC $(4.59MHz)$ and CP-PWC $(5.13MHz)$. Finally, the measurements of the $eSNR$ show that the best value is achieved by GC-PWC $(38dB)$, followed by OGC-PWC $(33dB)$ and CP-PWC $(21dB)$.

B. Cyst phantom results

In Fig.6 are showed the simulation B-mode images of the PICMUS cyst phantom. As it can be seen on these images, the three studied methods provide similar cyst qualities. Slight improvement $(0.2dB)$ provided by OGC-PWC compared to GC-PWC and CP-PWC can be observed on the second horizontal line of cysts. However, by looking at the speckle autocorrelation length (Fig.7), it can be seen that OGC-PWC yields $150\mu m$ (width at half height i.e. $-6dB$ on log scale) which is 16% better than CP-PWC $(175\mu m)$ and 50% better than GC $(225\mu m)$.

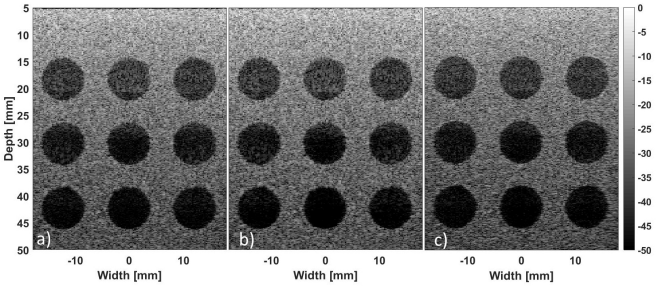

Fig. 6. B-mode images of the PICMUS cyst phantom, obtained using 9 plane wave coherent compounding for: a) - CP-PWC, b) - GC-PWC, d) - OGC-PWC

ISBN 978-90-827970-1-5 © EURASIP 2018

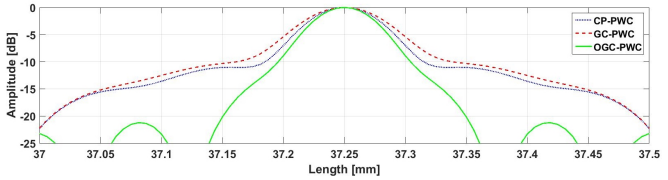

Fig. 7. Envelope of the speckle autocorrelation length computed on the cyst images obtained with the three methods studied. The measurements was performed on the vertical line at $x = -7mm$

IV. Experimental results

The experimental study was performed on a Gammex phantom (model 410SCG HE 0.5 Gammex Sun nuclear, Neu-Isenburg, Germany) using the open ultrasound platform UlaOp 256 (Microelectronics System Design Lab, Florence, Italy) [15]. A LA523E (Esaote, Genova, Italy) linear array probe, with 192 active elements of impulse response $h_{er}(t)$ illustrated in Fig.2d, was employed for plane wave emission/reception.

The obtained B-mode images are shown in Fig.8, where it can be visually assessed that the overall image quality of the OGC-PWC is better than the GC-PWC and CP-PWC image. The envelopes of the scatterer placed at $(x, z) = (-10, 19.6mm)$ ($100\mu m$ diameter) is presented in Fig.9a. A resolution of $201.1\mu m$ for OGC-PWC, $264.6\mu m$ for GC-PWC and $251.6\mu m$. These values correspond to a 25.1% boost of OGC-PWC compared to CP-PWC and a 32% boost of OGC-PWC compared to GC-PWC. The somehow diminished boost in resolution, compared to the expected theoretical/simulation values, can be explained by the fact that the OGC-PWC excitation signals are designed using a certain pulse-echo impulse response $h_{er}(t)$ supposed to be the same for all the elements, variations in $h_{er}(t)$ generating mismatches between the designed signal and the corresponding filter (in (11)) that result in resolution loss. The CNR measured from the anechoic cyst gives $2.4dB$, $6.1dB$ and $6.7dB$ for CP-PWC, GC-PWC and OGC-PWC respectively. The $eSNR$, measured on the received signals for CP-PWC and on the received signals after compression for GC-PWC and OGC-PWC, equals $15dB$ (CP-PWC), $35dB$ (GC-PWC) and $21dB$ (OGC-PWC).

V. Conclusion

In this paper, we propose a method that allows to adapt binary shift keyed Golay codes to the employed transducer, in order to increase the ultrasound image resolution. The new designed excitations are implemented in a coherent plane wave

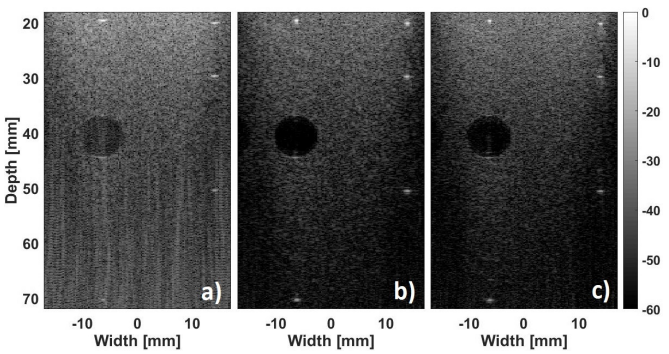

Fig. 8. B-mode images for: a) - CP-PWC, b) - GC-PWC, c) - OGC-PWC

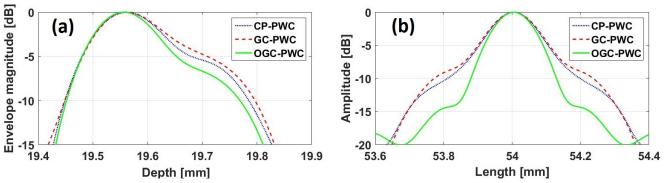

Fig. 9. a) - Envelope magnitude of the scatterer placed at $(x, z) = (-10, 19.6mm)$, b) - Envelope of the B-mode image speckle autocorrelation length obtained with the three methods studied. The measurements was performed on the vertical line at $x = 7mm$

compounding imaging method and their performance is studied in simulation and experimental setups. Clear improvements of the resolution, that follow the expected theoretical values, are obtained whilst echo to noise ratio and contrast to noise ratio are comparable to the classical coding scheme. As we showed in our theoretical study, the signal optimization does not depend on the emission beamforming scheme or binary code used, which proves its feasibility in various imaging approaches.

References

[1] J. A. Jensen, S. I. Nikolov, K. L. Gammelmark and M. H. Pedersen, "Synthetic aperture ultrasound imaging," Ultrasonics, vol. 44, Supplement, pp. e5-e15, 2006.

[2] C. Papadacci, M. Pernot, M. Couade, M. Fink, and M. Tanter, "High contrast ultrafast imaging of the heart," IEEE TUFFC, vol. 61, no. 2, pp. 288-301, 2014.

[3] G. Montaldo, M. Tanter, J. Bercoff, N. Benech, and M. Fink, "Coherent plane-wave compounding for very high frame rate ultrasonography and transient elastography," IEEE TUFFC, vol. 56, no. 3, pp. 489-506, 2009.

[4] H.Miwa, H. Hayashi, T. Shimura, K. Murakami, "Simultaneous multifrequency ultrasonography the principle and technology", IEEE IUS, pp. 655-659, 1981.

[5] F. Gran and J. A. Jensen, "Spatial encoding using a code division technique for fast ultrasound imaging," IEEE TUFFC, vol. 55, no. 1, pp. 12-23, 2008.

[6] D. Bujoreanu, H. Liebgott, and B. Nicolas,"Simultaneous coded plane wave imaging in ultrasound: Problem formulation and constraints," IEEE ICASSP, 2017.

[7] M. L. Oelze, "Bandwidth and resolution enhancement through pulse compression," IEEE TUFFC, vol. 54, no. 4. pp. 768-781, 2017.

[8] Y. M. Benane, R. Lavarello, D. Bujoreanu, C. Cachard, F. Varray, J. M. Escoffre, O. Basset, "Ultrafast ultrasound imaging using a resolution and bandwidth enhancement technique," IEEE IUS, pp. 1-4, 2017 .

[9] B. Lashkari, K. Zhang, A. Mandelis, "High-frame-rate synthetic aperture ultrasound imaging using mismatched coded excitation waveform engineering: A feasibility study," IEEE TUFFC, vol. 63 no.6, pp. 828-841, 2016.

[10] A. Nowicki, I. Trots, P. A. Lewin, W. Secomski, and R. Tymkiewicz, "Influence of the ultrasound transducer bandwidth on selection of the complementary Golay bit code length," Ultrasonics, vol. 47, nos. 14, pp. 64-73, 2007.

[11] R. Y. Chiao, L. J. Thomas, "Synthetic transmit aperture imaging using orthogonal golay coded excitation," IEEE IUS, vol. 2, pp. 1677-1680, 2000.

[12] F. Zhao, L. Tong, Q. He, J. Luo, "Coded excitation for diverging wave cardiac imaging: a feasibility study," PMB, vol. 62, no. 4, p. 1565, 2017.

[13] J. A. Jensen, "Field: A program for simulating ultrasound systems," in 10th Nordicbaltic Conference on Biomedical Imaging, supplement 1, part 1, vol. 4, pp. 351-353, 1996.

[14] H. Liebgott, A. R-Molares, J. A. Jensen, O. Bernard, "Plane-Wave Imaging Challenge in Medical Ultrasound", IEEE IUS, pp. 1-4, 2016.

[15] E. Boni, L. Bassi, A. Dallai, F. Guidi, V. Meacci, A. Ramalli, P. Tortoli, "ULA-OP 256: A 256-channel open scanner for development and real-time implementation of new ultrasound methods," IEEE TUFFC, vol. 63, no. 10, pp. 1488-1495, 2016.

ISBN 978-90-827970-1-5 © EURASIP 2018